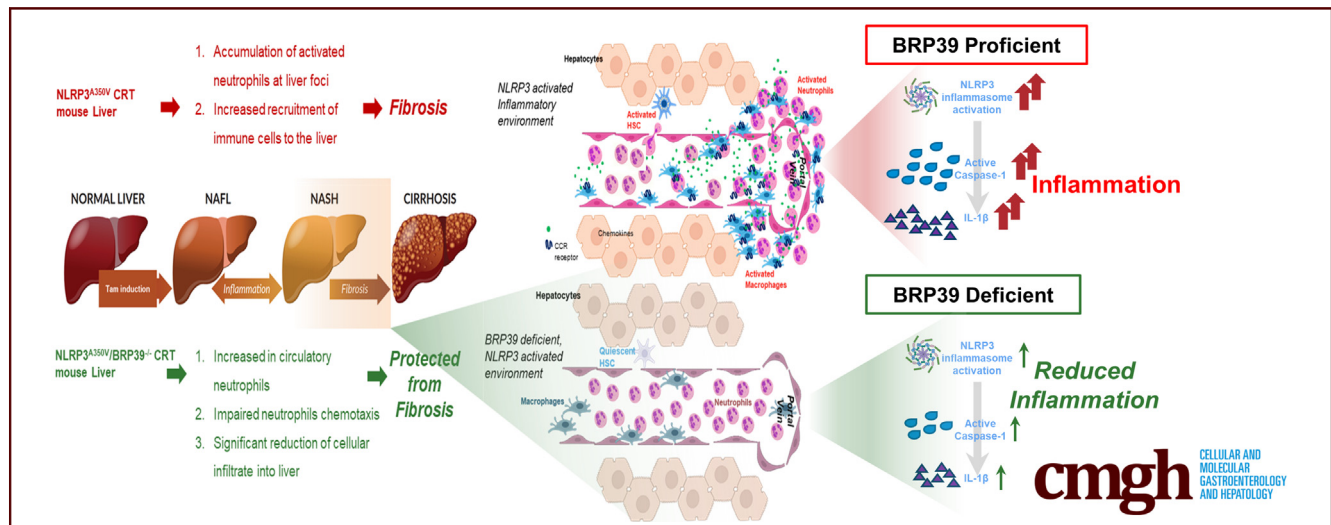


ORIGINAL RESEARCH

BRP39 Regulates Neutrophil Recruitment in NLRP3 Inflammasome-Induced Liver Inflammation

Lin Kui,¹ Andrea D. Kim,^{1,2} Janset Onyuru,¹ Hal M. Hoffman,¹ and Ariel E. Feldstein^{1,3}¹Department of Pediatrics, University of California San Diego, San Diego, California; ²Department of Surgery, Johns Hopkins University, Baltimore, Maryland; and ³Global Drug Discovery, Novo Nordisk, Denmark

SUMMARY

The effect of breast regression protein 39 deficiency in modulating Nucleotide oligomerization domain (NOD)-like-receptor protein 3 inflammasome during liver inflammation and nonalcoholic steatohepatitis fibrosis, influencing cellular activation, recruitment, and infiltration of macrophages and neutrophils, was characterized.

BACKGROUND & AIMS: Breast regression protein 39 (BRP39) (Chi3L1) and its human homolog YKL-40, is an established biomarker of liver fibrosis in nonalcoholic steatohepatitis (NASH) patients, but its role in NASH pathogenesis remains unclear. We recently identified Chi3L1 as one of the top up-regulated genes in mice with inducible gain-of-function NOD-like receptor protein 3 (NLRP3) activation that mimics several liver features of NASH. This study aimed to investigate the effects of BRP39 deficiency on NLRP3-induced liver inflammation using tamoxifen-inducible *Nlrp3* knockin mice sufficient (*Nlrp3*^{A350V} CRT) and deficient for BRP39 (*Nlrp3*^{A350V}/BRP^{-/-} CRT).

METHODS: Using *Nlrp3*^{A350V} CRT mice and *Nlrp3*^{A350V} BRP^{-/-} CRT, we investigated the consequences of BRP39 deficiency influencing NLRP3-induced liver inflammation.

RESULTS: Our results showed that BRP39 deficiency in NLRP3-induced inflammation improved body weight and liver weight. Moreover, liver inflammation, fibrosis, and hepatic stellate cell

activation were reduced significantly, corresponding to significantly decreased Ly6C⁺ infiltrating macrophages, CD68⁺ osteopontin-positive hepatic lipid-associated macrophages, and activated Lymphocyte antigen 6 complex locus G6D positive (Ly6G⁺) and citrullinated histone H3 positive (H3Cit⁺) neutrophil accumulation in the liver. Further investigation showed that circulatory neutrophils from NLRP3-induced BRP39-deficient mice have impaired chemotaxis and migration ability, and this was confirmed by RNA bulk sequencing showing reduced immune activation, migration, and signaling responses in neutrophils.

CONCLUSIONS: These data showcase the importance of BRP39 in regulating the NLRP3 inflammasome during liver inflammation and fibrotic NASH by altering cellular activation, recruitment, and infiltration during disease progression, and revealing BRP39 to be a potential therapeutic target for future treatment of inflammatory NASH and its associated diseases. (*Cell Mol Gastroenterol Hepatol* 2024;17:481–497; <https://doi.org/10.1016/j.jcmgh.2023.12.002>)

Keywords: NASH; LAMs; LY6G; Fibrosis.

Nonalcoholic fatty liver disease (NAFLD) is a multifaceted disease, spanning from minimal inflammatory activity and no evidence of cell damage, referred to as non-nonalcoholic steatohepatitis (NASH) fatty liver, to NASH, with the latter classified by severe inflammation, leading to hepatocellular injury (hepatocyte ballooning), steatosis with different degrees of fibrosis,^{1,2} liver cirrhosis,

end-stage liver disease, and hepatocellular carcinoma. With the global obesity epidemic of the 21st century, NAFLD now is recognized as the most frequent cause of chronic liver disease in both adults and children worldwide.³ Currently, there are no approved therapies for the treatment of NASH, with NASH being a leading indication for liver transplantation.⁴⁻⁶

Breast regression protein 39 (BRP39; chitinase-3-like protein 1 [Chi3L1]) and its human homolog YKL-40 is a glycoprotein expressed by various cell types including macrophages, neutrophils, fibroblasts, and epithelial cells. The mechanistic role of BRP39 was first described in the lungs, whereby the interleukin (IL)1 family of cytokines induce BRP39 production,^{7,8} and enhance Type 2 helper T cells response by increasing expression of IL4, IL5, and IL13 cytokines,⁹ in a interleukin-13 receptor $\alpha 2$ (IL13R $\alpha 2$)-dependent manner.¹⁰ BRP39 activates dendritic cells and macrophages, while inhibiting inflammatory cell Fas-mediated apoptosis, by up-regulating protein kinase B/AKT and Fas apoptotic inhibitory molecule 3 (Faim3).¹¹ Recently, YKL-40 was proposed as a prognostic biomarker and therapeutic target in conditions characterized by acute or chronic inflammation, extracellular matrix remodeling, fibrosis, and cancer.¹²⁻¹⁶ Serum YKL-40 is a well-established biomarker of liver fibrosis in NASH patients,¹⁷⁻¹⁹ whereas the potential mechanistic contribution to NASH pathogenesis remains poorly understood.

Our group has shown that NOD-like receptor protein 3 (NLRP3) inflammasome activation is essential in NASH progression, which is up-regulated in livers of patients with NASH.²⁰ We also recently identified BRP39 as one of the top up-regulated genes in the livers of mice with inducible gain-of-function Nlrp3 activation, which mimics several liver features of NASH.²¹ Thus, Nlrp3^{A350V} activated mice serve as a foundation to study inflammasome-driven liver inflammation and fibrosis, and the potential therapeutic effect of BRP39 modulation. In the present study, we evaluated the effect of BRP39 deficiency in reducing the development of inflammation and fibrosis in mice with gain-of-function NLRP3 mutations. We show that knocking out BRP39 in NLRP3-hyperactivated mice reduces liver inflammation and fibrogenesis, and decreases infiltrating lipid-associated macrophages (LAMs) and neutrophils, 2 immune cells that play key roles in NASH progression.

Results

Inducible Knockout of BRP39 in NLRP3-Activated Mice Shows Improvement of Liver Weight With Liver Regeneration


In our previous study, we showed that Chi3L1 (BRP39) is one of the top up-regulated genes in murine liver with inducible gain-of-function NLRP3 activation, which mimics several pathogenetic features of NASH.²¹ Therefore, we investigated whether deleting BRP39 would improve the disease outcome of NLRP3-mediated liver inflammation in mice. To study the consequence of BRP39 deficiency in NLRP3-activation-driven liver pathogenesis, we generated tamoxifen-inducible Nlrp3^{A350V} CRT mice on a conditional BRP (CHI3L1) knockout background. Tamoxifen-inducible NLRP3 knockin Nlrp3^{A350V} CRT mice were used as positive controls, and CRT-negative mice were used as WT

controls. Mice at 7 weeks of age were given 3 successive doses of tamoxifen by intraperitoneal injection, 1 on each day, for a total of 3 days and killed at week 10 for tissue and blood analysis (study design shown in Figure 1A). We confirmed the efficiency of tamoxifen-induced knockout of Brp39 by quantitative polymerase chain reaction (PCR) (Figure 2A) and Western blot (Figure 2B) of whole liver lysate. As shown previously, Nlrp3^{A350V} CRT mice appeared sick with signs of systemic inflammation and significant weight loss (Figure 1B), as well as an increased liver/body weight ratio (Figure 1D) after NLRP3 activation, compared with wild-type (WT) controls. In contrast, Nlrp3^{A350V}/BRP^{-/-} CRT mice have similar body weight (Figure 1B) and liver weight (Figure 1D) as WT mice. Because we observed a significant increase in the liver/body weight ratio (Figure 1C) in Nlrp3^{A350V}/BRP^{-/-} CRT compared with WT mice, we performed a whole-liver gene expression analysis and found significant up-regulation of Ki67 gene expression (Figure 1E), suggesting liver regeneration. Taken together, these data suggest that NLRP3-mediated inflammatory liver pathogenesis is improved in the absence of BRP39.

BRP39 Deficiency in NLRP3-Activated Mice Results in Significant Reduction of Hepatic Stellate Cell Activation and Liver Fibrosis

Previous studies by our group have shown that NLRP3 activation resulted in liver inflammation leading to fibrosis development.^{20,22,23,24} Similarly, we saw a significant increase in collagen deposition (Figure 3A and B) ($P < .05$) and α -smooth muscle actin (α -SMA) expression (Figure 3C and D) ($P < .01$) in immunohistochemical (IHC)-stained liver tissue, and an increase in messenger RNA (mRNA) expression of markers of hepatic stellate cell (HSC) activation, transforming growth factor- β (7-fold increase compared with WT; $P < .05$) and ACTA2 (17-fold; $P < .05$), and fibrosis markers, Col1a1 (10-fold, $P < .0001$), connective tissue growth factor (7-fold; $P < .001$), and tissue inhibitor of metalloproteinases 1 (50-fold; $P < .01$) in whole liver of Nlrp3^{A350V} CRT mice (Figure 3E) compared with WT. To

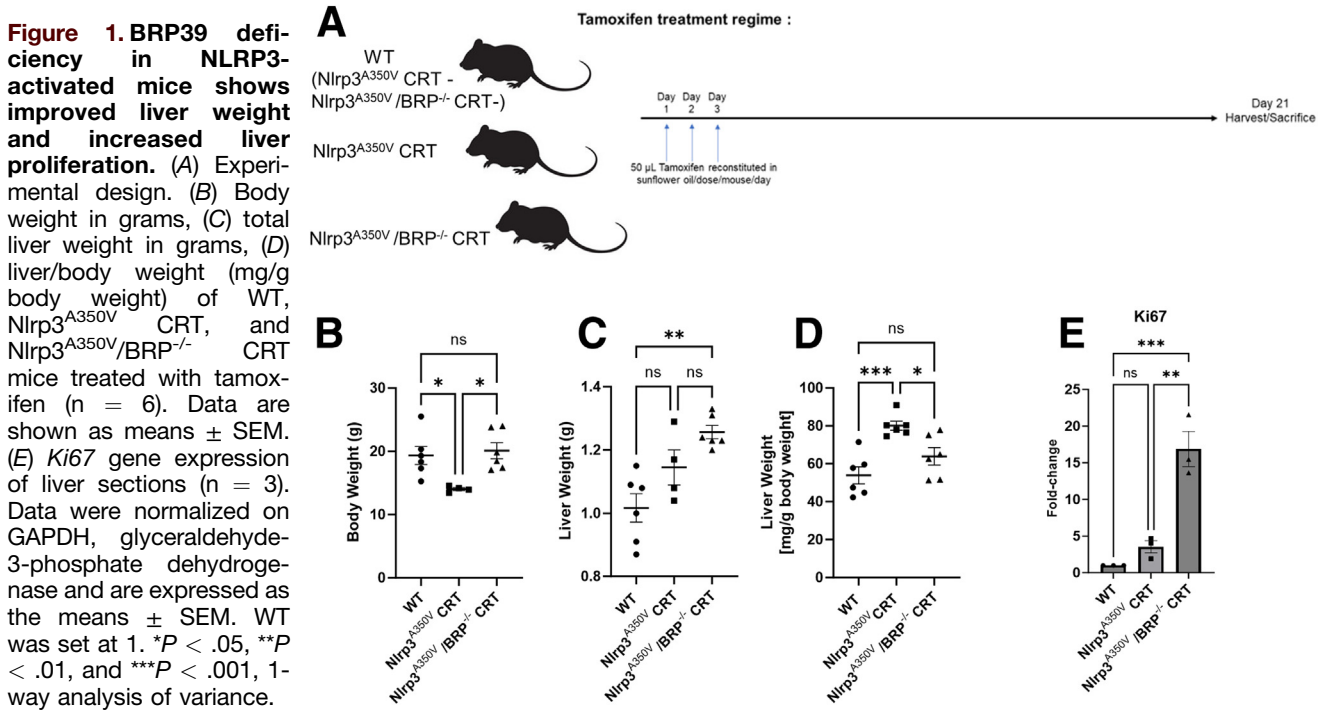
Abbreviations used in this paper: α -SMA, α -smooth muscle actin; BMDM, bone marrow-derived macrophage; BRP39, breast regression protein 39; BRP39 CRT, mice with myeloid lineage-specific knockout of BRP39; CCL, cc chemokine ligands; Chi3L1, chitinase-3-like protein 1; CM, complete medium; CXCL, The chemokine (C-X-C motif) ligand; FBS, fetal bovine serum; HRP, horseradish peroxidase; HSC, hepatic stellate cell; IF, Immunofluorescence; IHC, immunohistochemistry; IL, interleukin; LAM, lipid-associated macrophage; LPS, lipopolysaccharide; LSEC, liver sinusoidal endothelial cell; Ly6C, lymphocyte antigen 6 complex, locus C1; Ly6G, lymphocyte antigen 6 family member G; mRNA, messenger RNA; NAFLD, nonalcoholic fatty liver disease; NASH, nonalcoholic steatohepatitis; NLRP3, NOD-like receptor protein 3; Nlrp3^{A350V} CRT, tamoxifen-inducible Nlrp3 knockin mice; Nlrp3^{A350V}/BRP^{-/-} CRT, tamoxifen-inducible Nlrp3 knockin BRP39-deficient mice; OPN, osteopontin; PBS, phosphate-buffered saline; PCR, polymerase chain reaction; WT, wild-type.

 Most current article

© 2023 The Authors. Published by Elsevier Inc. on behalf of the AGA Institute. This is an open access article under the CC BY-NC-ND license (<http://creativecommons.org/licenses/by-nc-nd/4.0/>).

2352-345X

<https://doi.org/10.1016/j.jcmgh.2023.12.002>

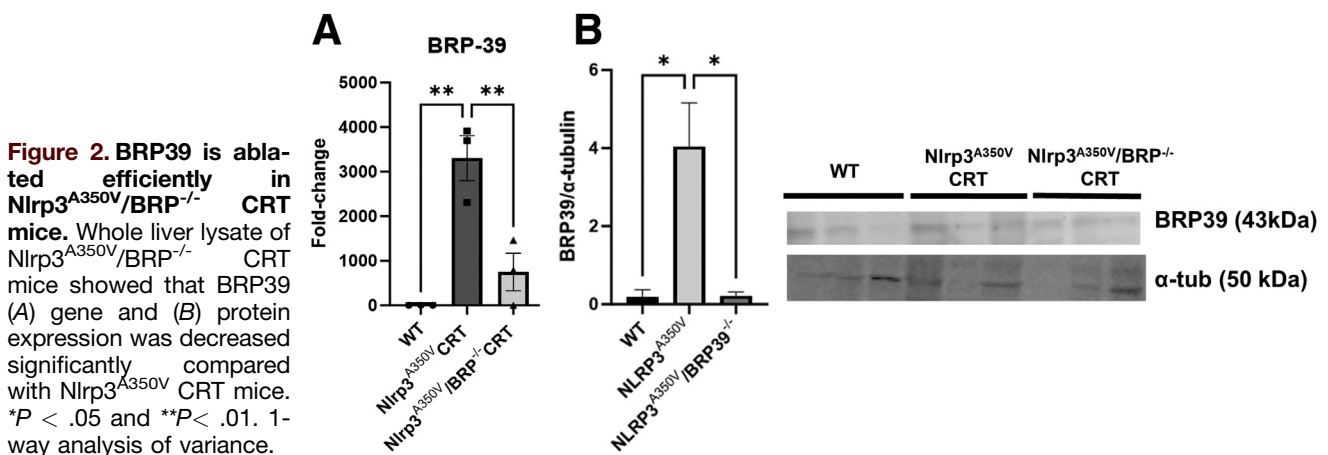


evaluate the role of BRP39 in NLRP3-mediated liver fibrosis, we performed the same analysis on the Nlrp3^{A350V}/BRP^{-/-} CRT mice and found a significant reduction of collagen deposition in the Sirius red-stained liver tissue (Figure 3A and B) (P < .05), and a significant decrease of α-SMA expression (Figure 3C and D) (P < .05) in IHC-stained liver biopsy specimens of Nlrp3^{A350V}/BRP^{-/-} CRT compared with Nlrp3^{A350V} CRT mice, suggesting a diminished activation state of HSCs. The gene expression of fibrosis markers transforming growth factor-β (4-fold decrease compared with Nlrp3^{A350V} CRT; P < .05), ACTA2 (16-fold; P < .05), Col1a1 (8-fold; P < .0001), profibrotic connective tissue growth factor (4.5-fold; P < .001), and tissue inhibitor of metalloproteinases 1 (30-fold; P < .05) also were reduced significantly in Nlrp3^{A350V}/BRP^{-/-} CRT mice liver compared with Nlrp3^{A350V}

CRT mice (Figure 3E). These data suggest that liver fibrosis and HSC activation driven by NLRP3 inflammasome activation is dependent on the function of BRP39.

BRP39 Deficiency in NLRP3-Activated Mice Leads to Reduction in Caspase 1 Activation and Inflammatory Cytokine Expression in the Liver

Formation of the NLRP3 inflammasome drives caspase-1 activation, which leads to a cascade of inflammatory cytokine release including IL1β. To study the effect of BRP39 deficiency on NLRP3-mediated inflammation, we investigated the mRNA gene expression and protein levels of NLRP3 inflammasome components and downstream mediators. Gene expression of NLRP3 (12-fold increase compared with



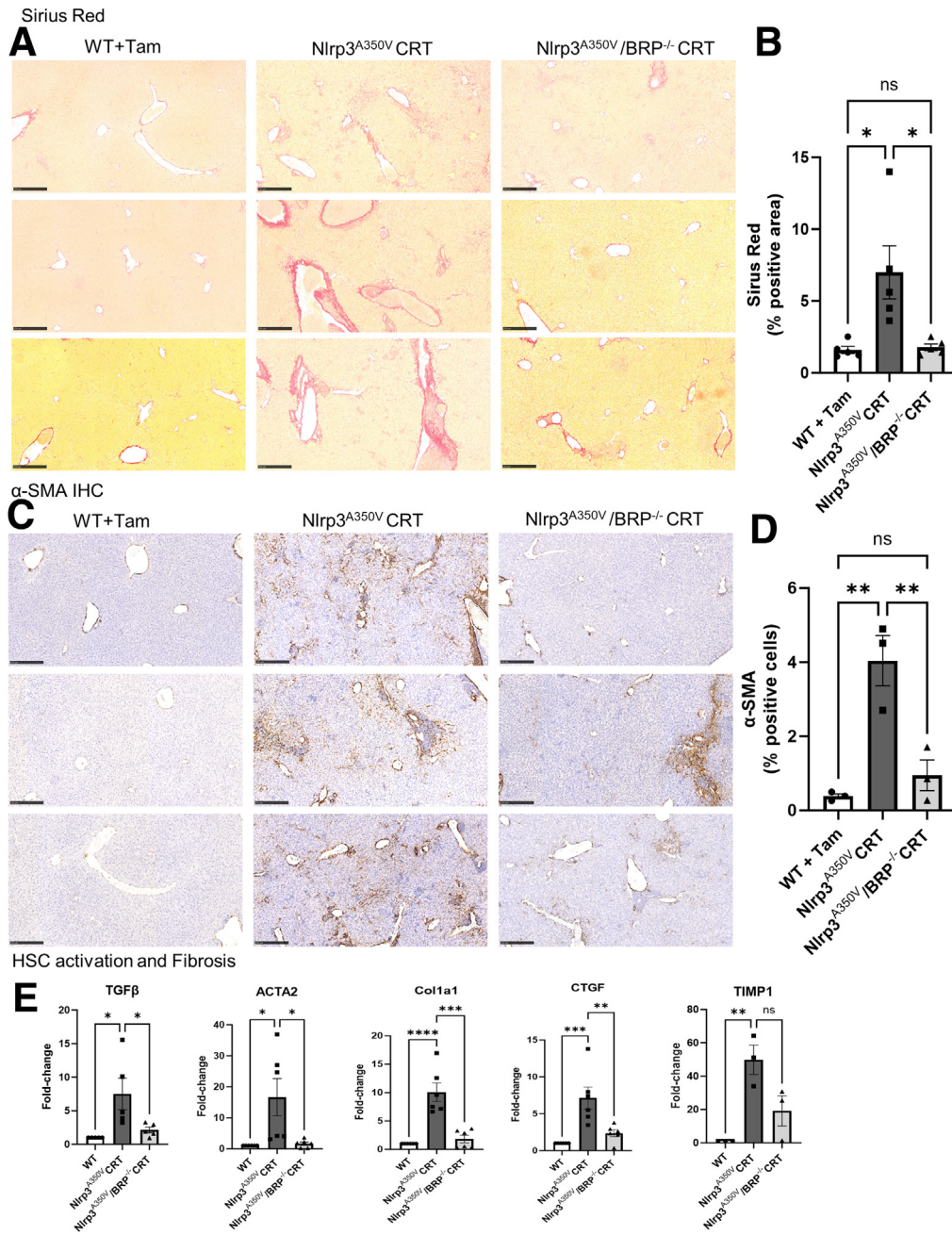


Figure 3. BRP39 deficiency in NLRP3-activated mice ameliorates liver fibrosis. HSC activation markers collagen (A and B) and α -SMA (C and D) were detected in liver paraffin-embedded sections of Nlrp3^{A350V} CRT mice and decreased in Nlrp3^{A350V}/BRP^{-/-} CRT mice. $n \geq 3$ mice per genotype. Scale bar: 250 μ m. (E) mRNA expression of HSC activation markers (TGF β and ACTA2) and fibrosis markers (CTGF, Col1a1, and TIMP1) were increased in Nlrp3^{A350V} CRT compared with WT, and significantly decreased in Nlrp3^{A350V}/BRP^{-/-} CRT compared with Nlrp3^{A350V} CRT whole liver tissue ($n \geq 3$ for each group). Data were normalized on GAPDH, glyceraldehyde-3-phosphate dehydrogenase and are expressed as the means \pm SEM. WT was set at 1. * $P < .05$, ** $P < .01$, *** $P < .001$, and **** $P < .0001$, 1-way analysis of variance. CTGF, connective tissue growth factor.

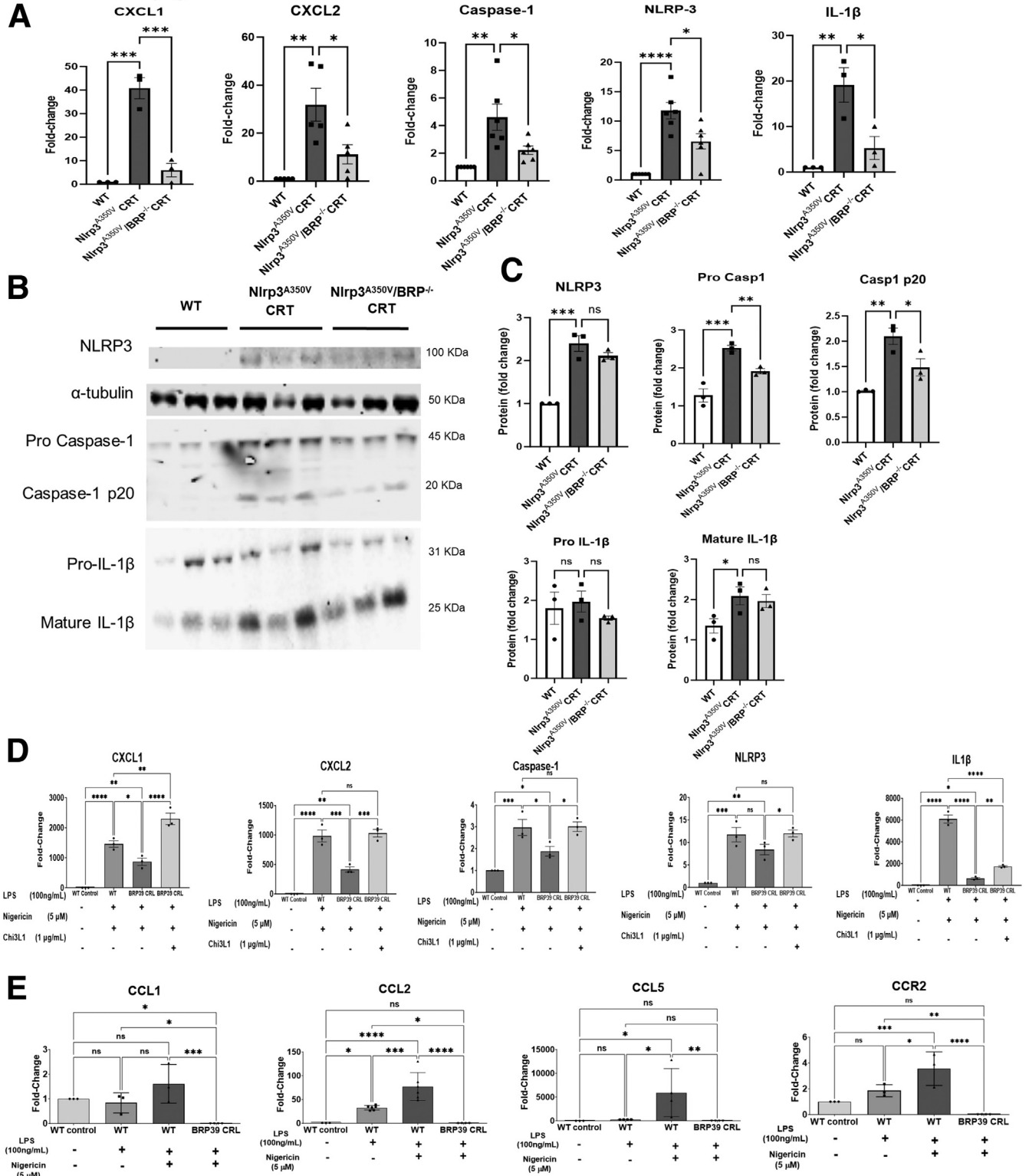
WT control; $P < .0001$), *IL1 β* (19-fold; $P < .01$), *caspase-1* (4.1-fold; $P < .01$), *CXCL-1* (40-fold; $P < .0001$), and *CXCL-2* (32-fold; $P < .001$) (Figure 4A) were up-regulated in whole livers of Nlrp3^{A350V} CRT mice compared with WT mice. Induced knockout of BRP39 in Nlrp3^{A350V}/BRP^{-/-} CRT mice significantly decreased these inflammatory genes (*NLRP3* [6-fold decrease compared with Nlrp3^{A350V} CRT; $P < .05$], *IL1 β* [14-fold; $P < .05$], *caspase-1* [(1.9-fold; $P < .05$), *CXCL-1* [32-fold; $P < .0001$], *CXCL-2* [22-fold; $P < .05$]) in whole liver, to an expression level comparable with WT controls. We confirmed the efficiency of the tamoxifen Cre-dependent deletion on Brp39 gene expression (2200-fold; $P < .01$)

(Figure 4A). NLRP3 inflammasome formation leads to activation of caspase-1 and subsequent maturation and secretion of inflammatory cytokines such as IL1 β . With Western blot analysis of whole-liver protein lysate (Figure 4B), we observed significantly higher post-translational protein expression of pro-caspase-1 (1.3-fold increase compared with WT control; $P < .001$), cleaved caspase-1 (1.1-fold; $P < .01$), and mature IL1 β (0.8-fold; $P < .05$) in whole liver from Nlrp3^{A350V} CRT mice compared with the WT controls. Conditional BRP39 deficiency in NLRP3-activated mice did not have a significant effect on expression at the protein level of NLRP3, pro-IL1 β , or mature IL1 β , however, it significantly

reduced pro-caspase-1 (0.6-fold decrease compared with Nlrp3^{A350V} CRT; $P < .01$) and cleaved caspase-1 (0.6-fold; $P < .05$) expression (Figure 4B and C). Because NLRP3-activated infiltrating macrophages are a key contributor

aggravating NAFLD, we investigated if BRP39 deficiency in macrophages would affect NLRP3-activated inflammation by comparing inflammatory gene expression between lipopolysaccharide (LPS) (100 ng/mL) and nigericin (5 μ mol/L)

Inflammatory gene



activated bone marrow-derived macrophages (BMDMs) of WT and myeloid cell-specific BRP39 knockout mice (BRP39^{-/-} CRL). Gene expression of *CXCL-1* (1500-fold increase compared with WT unstimulated control; $P < .0001$), *CXCL-2* (1000-fold; $P < .0001$), *caspase-1* (3-fold; $P < .001$), *NLRP3* (12-fold; $P < .001$), and *IL1 β* (6000-fold; $P < .0001$) (Figure 4D) were up-regulated in NLRP3-activated WT BMDMs compared with unstimulated controls. NLRP3-activated BRP39^{-/-} CRL BMDMs have significantly reduced expression of these inflammatory genes (*CXCL-1* [1.7-fold; $P < .05$], *CXCL-2* [2.1-fold; $P < .001$], *caspase-1* [1.5-fold; $P < .05$], *NLRP-3* [1.5-fold; $P < .01$], and *IL1 β* [11-fold; $P < .0001$]) compared with stimulated WT BMDMs. Interestingly, pretreatment with 1 μ g recombinant Mouse Chitinase 3-like 1 (rmChi3L1) protein overnight, followed by NLRP3 activation in BRP39^{-/-} CRL BMDMs, restored the inflammatory gene activation to a level comparable with that of NLRP3-activated WT (*CXCL-1* [2.2-fold; $P < .0001$], *CXCL-2* [1.7-fold; $P < .01$], *caspase-1* [2.1-fold; $P < .05$], *NLRP3* [1.5-fold; $P < .05$], and *IL1 β* [3.3-fold; $P < .01$]) compared with stimulated BRP39^{-/-} CRL BMDMs. Because we found that BRP39 deficiency affected NLRP3-mediated inflammatory gene activation in macrophages, next we asked if its chemotactic ability also would be affected by comparing chemokines and chemokine-receptor gene expression of NLRP3-activated WT and BRP39^{-/-} CRL BMDMs. Chemokines (C-C motif) ligand 1 (*CCL1*) (1.5-fold; $P = .1083$), *CCL2* (75-fold; $P < .0001$), *CCL5* (500-fold; $P < .05$), and chemokine-receptor *CCR2* (3.5-fold; $P < .001$) gene expression (Figure 4E) are up-regulated in WT BMDMs treated with LPS (100 ng/mL) and nigericin (5 μ mol/L) compared with untreated WT controls. On the contrary, BRP39 deficiency in macrophages would significantly dampen the expression of chemokine (*CCL1*, $P < .001$; *CCL2*, $P < .0001$; and *CCL5*, $P < .01$) gene expression >1 fold, and chemokine-receptor *CCR2* (gene expression >1 fold; $P < .0001$) compared with activated WT BMDMs.

Collectively, our data showed that reduction of BRP39 in NLRP3-activated inflammation decreased inflammasome activation by reducing pro-caspase-1 expression and caspase-1 production, and diminished macrophage activation, migration, and recruitment ability, leading to a dampened inflammatory environment in the liver.

BRP39 Deficiency in NLRP3-Activated Mice Diminishes the Accumulation of Macrophages in Liver

Activated macrophages play an important role in the disease progression of NAFLD. Remmerie et al²⁵ have described a specific phenomenon in NAFLD liver whereby Kupffer cells, the liver resident macrophages, are reduced, and replaced by 2 major subsets of infiltrating bone marrow-derived macrophages, Kupffer-like macrophages and LAMs. These LAMs express osteopontin (OPN) and are associated with liver fibrosis in NASH patients. Liver tissues from WT, Nlrp3^{A350V} CRT, and Nlrp3^{A350V}/BRP^{-/-} CRT mice (Figure 5A and B) did not show any significant difference by IHC staining of F4/80-expressing macrophages. However, we found a significant increase in Immunofluorescence (IF) staining of lymphocyte antigen 6 complex, locus C1 (Ly6C)-expressing bone marrow macrophage (Figure 5A and C) ($P < .0001$) and CD68-positive, OPN-positive LAMs (Figure 5E and D) ($P < .001$) in Nlrp3^{A350V} CRT mice livers compared with WT control. Induced BRP39 deficiency in NLRP3 activated mice resulted in significantly reduced numbers of bone marrow macrophage (Figure 5A and C) (percentage of Ly6C-positive cells 3 times lower than Nlrp3^{A350V} CRT; $P < .0001$) and LAM infiltration (Figure 5E and D) (percentage of CD68+OPN+ cells 3 times lower; $P < .01$) into the liver. Taken together, our data showed that BRP39 deficiency reduced infiltration and accumulation of activated bone marrow macrophages and LAMs in the liver, contributing toward quelling liver inflammation and fibrosis.

BRP39 Deficiency in NLRP3-Activated Mice Significantly Reduced Neutrophil Recruitment and Activation in the Liver

During the inflammatory phase of NAFLD, neutrophils are the first responders recruited to the site, which consequently promotes the recruitment of other proinflammatory leukocytes, exacerbating the inflammatory microenvironment. In our study, we found that NLRP3 activation in mice increased infiltration and accumulation of Lymphocyte antigen 6 complex locus G6D (Ly6G)-positive neutrophils at liver foci ($P < .001$) of Nlrp3^{A350V} CRT mice compared with WT controls. Consequently, conditional BRP39 deficiency during

Figure 4. (See previous page). **BRP39 deficiency in NLRP3-activated mice reduced inflammatory expression in whole liver and macrophages.** (A) The inflammatory mRNA gene expression of *CXCL1*, *CXCL2*, *caspase-1*, *BRP39*, *NLRP-3*, and *IL1 β* was increased significantly in Nlrp3^{A350V} CRT compared with WT, and decreased in Nlrp3^{A350V}/BRP^{-/-} CRT whole liver lysate compared with Nlrp3^{A350V} CRT. $n > 3$ per group. (B and C) Protein expression of *NLRP3*, *Pro Casp1*, *Casp1 p20*, *Pro IL1 β* , and mature *IL1 β* ($n = 3$ mice per genotype for Western blot) of whole-liver lysate were analyzed using Western blot, showing a significant decrease of caspase-1 and p20 caspase-1 in Nlrp3^{A350V}/BRP^{-/-} CRT compared with Nlrp3^{A350V} CRT. (D) The inflammatory mRNA gene expression of *CXCL1*, *CXCL2*, *caspase-1*, *NLRP-3*, and *IL1 β* was increased significantly in LPS and nigericin-stimulated WT BMDM compared with unstimulated control, decreased in stimulated BRP39 CRL BMDM compared with stimulated WT BMDM, and addition of 1 μ g/mL recombinant mouse Chi3L1 (BRP39) protein followed by LPS and nigericin stimulation in BRP39 CRL BMDM increased the inflammatory gene expression significantly compared with NLRP3-activated BRP39 CRL. (E) Chemokines *CCL1*, *CCL2*, *CCL5*, and chemokine receptor *CCR2* expression were increased significantly in LPS and nigericin-stimulated WT BMDM compared with untreated WT control or WT treated with LPS alone, and significantly absent in NLRP3-activated BRP39 CRL BMDM. mRNA gene expressions were normalized on GAPDH, glyceraldehyde-3-phosphate dehydrogenase and are expressed as the means \pm SEM. WT was set at 1. Protein fold change is defined as signal of sample in Nlrp3^{A350V} CRT or Nlrp3^{A350V}/BRP^{-/-} CRT normalized to α -tubulin, over signal of WT normalized to α -tubulin, and are expressed as the means \pm SEM. * $P < .05$, ** $P < .01$, *** $P < .001$, and **** $P < .0001$, 1-way analysis of variance.

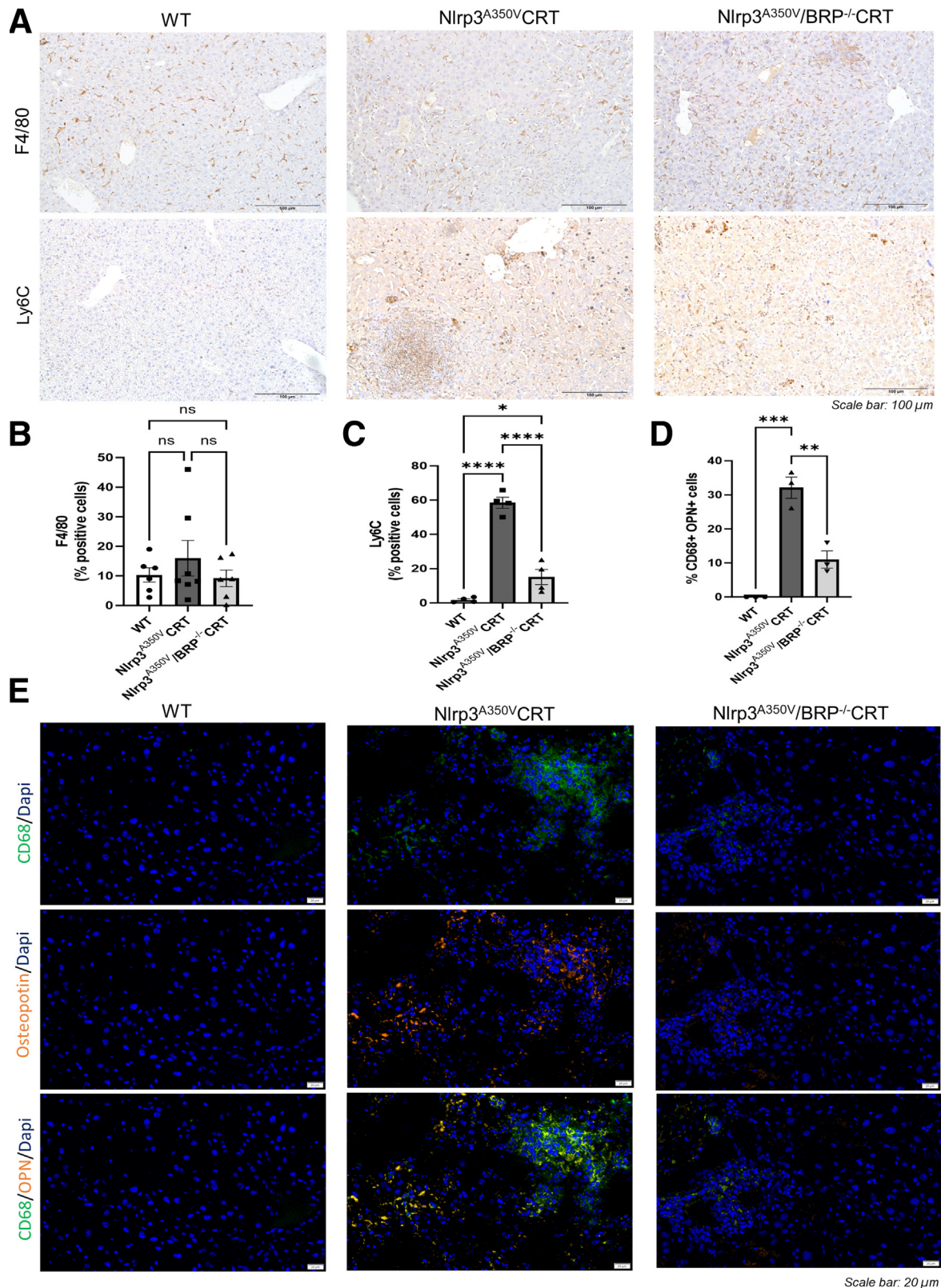


Figure 5. BRP39 deficiency in NLRP3-activated mice reduced osteopontin-positive infiltrating myeloid cells in the whole liver. (A and B) IHC staining with F4/80 (scale bar: 100 μ m) showed no significant differences of total macrophages between the different groups but Ly6C (A, scale bar: 100 μ m) revealed a significant increase of inflammatory macrophages in Nlrp3^{A350V} CRT compared with WT, and a significant decrease in Nlrp3^{A350V}/BRP^{-/-} CRT compared with Nlrp3^{A350V} CRT liver (C). IF staining with CD68 and osteopontin (E) (scale bar: 20 μ m) showed an increase in (D) infiltrating LAM in Nlrp3^{A350V} CRT vs WT, but decreased LAM in Nlrp3^{A350V}/BRP^{-/-} CRT vs Nlrp3^{A350V} CRT. $n \geq 3$ mice per genotype, representative images are shown. Data are expressed as the means \pm SEM. * $P < .05$; ** $P < .01$; *** $P < .001$; **** $P < .0001$, 1-way analysis of variance. DAPI, 4',6-diamidino-2-phenylindole.

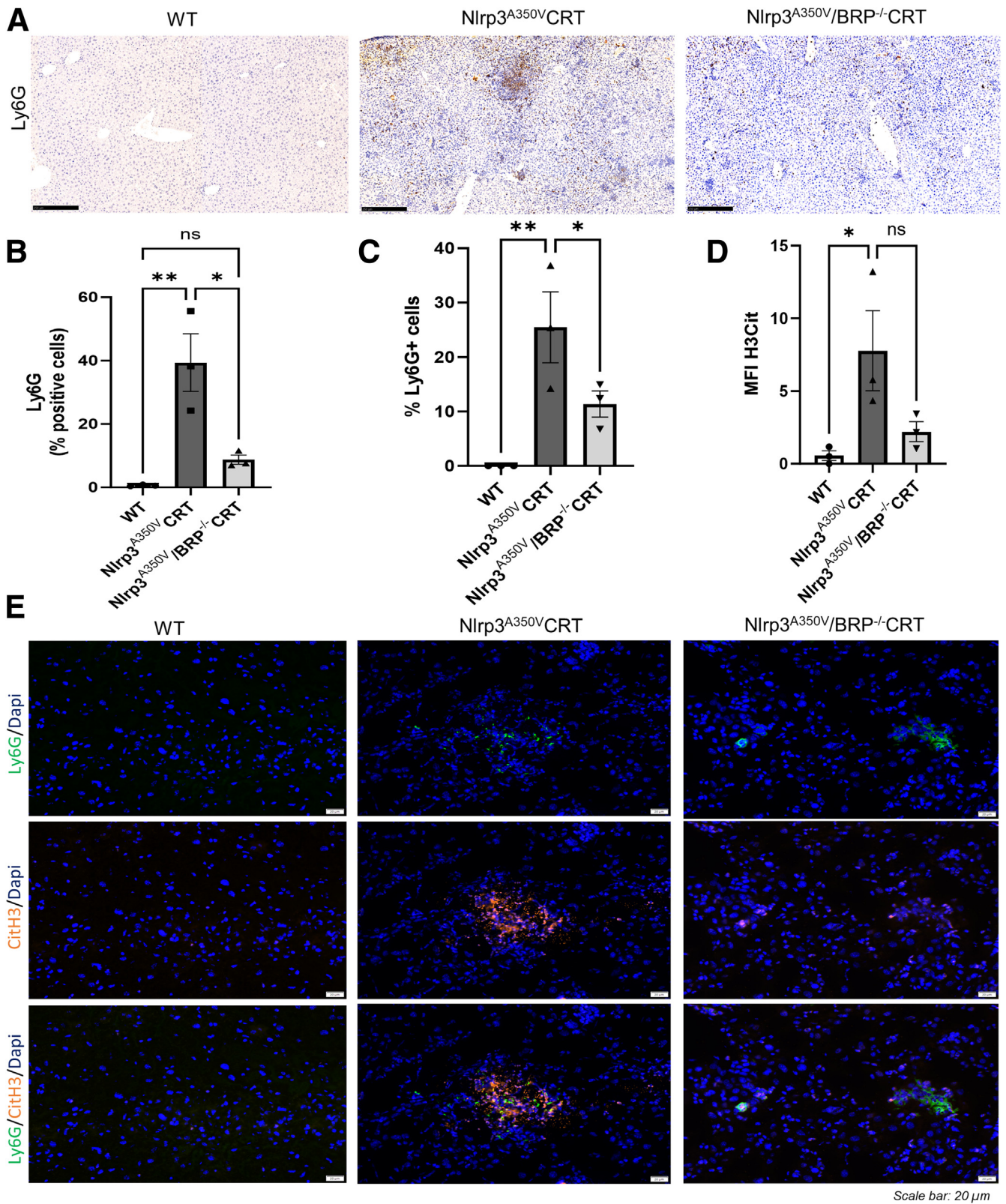


Figure 6. BRP39 deficiency in NLRP3-activated mice decreased neutrophil accumulation and activation in the whole liver. (A) IHC staining with Ly6G (scale bar: 250 μ m) (B) Histogram showing a significant increase of infiltrated neutrophils (% Ly6G+ cells) in Nlrp3^{A350V} CRT compared with WT, and a significant decrease in Nlrp3^{A350V}/BRP^{-/-} CRT compared with Nlrp3^{A350V} CRT liver (C) Histogram showing IF staining of % Ly6G+ cells (D) Histograms showing MFI of IF H3Cit staining (scale bar: 20 μ m) (E) IF staining with Ly6G and CitH3. Data are expressed as the means \pm SEM. **P* < .05, ***P* < .01, 1-way analysis of variance. DAPI, 4',6-diamidino-2-phenylindole.

NLRP3 activation significantly reduced the accumulation of neutrophils in liver foci (Figure 6A and B) ($P < .05$) of $Nlrp3^{A350V}/BRP^{-/-}$ CRT mice compared with $Nlrp3^{A350V}$ CRT, as shown by IHC staining of liver. Moreover, IF staining (Figure 6E) showed that the activation state of neutrophils, signified by Citrullinated histone H3 (H3Cit) (Figure 6D) mean fluorescent intensity in liver, was increased in $Nlrp3^{A350V}$ CRT ($P < .01$) when compared with WT control, and drastically decreased in $Nlrp3^{A350V}/BRP^{-/-}$ CRT mice ($P < .05$) when compared with $Nlrp3^{A350V}$ CRT. Collectively, we saw that BRP39 deficiency in NLRP3-activated mice drastically reduced recruitment and activation of neutrophils in the liver.

Conditional BRP39 Knockout in NLRP3-Activated Mice Resulted in Impaired Neutrophil Migration

Because we saw a remarkable reduction of activated neutrophils in BRP39-deficient NLRP3-activated mice livers, we next investigated whether this phenomenon was the result of the reduction of total circulating neutrophils in whole blood, or its migration ability. We collected whole blood from mice by cardiac puncture and performed hematology analysis with the Veterinary hematology analyzer Scil Vet abc (Scil Animal Care, France). We observed an increase in absolute white blood cells ($P < .001$) and granulocytes ($P < .0001$) in whole blood from $Nlrp3^{A350V}$ CRT mice compared with WT control mice (Figure 7A). Unexpectedly, we found increased white blood cell ($P < .01$) and granulocyte counts ($P < .05$) in $Nlrp3^{A350V}/BRP^{-/-}$ CRT mice when compared with NLRP3-activated mice ($Nlrp3^{A350V}$ CRT) with normal BRP39 expression (Figure 6A). Further analysis of whole blood with flow staining of CD11b and Ly6G antibodies confirmed that $Nlrp3^{A350V}/BRP^{-/-}$ CRT mice have increased circulating neutrophils in whole blood compared with $Nlrp3^{A350V}$ CRT mice ($P < .05$) (Figure 7B). The increased number of circulating CD11b+ Ly6G+ neutrophils in $Nlrp3^{A350V}/BRP^{-/-}$ CRT whole blood did not correspond with the reduced Ly6G+ neutrophil infiltrate we saw in the livers compared with $Nlrp3^{A350V}$ CRT mice. This observation suggests that neutrophil chemotaxis of $Nlrp3^{A350V}/BRP^{-/-}$ CRT mice could be dysfunctional. Thus, we compared the migration ability of WT, $Nlrp3^{A350V}$ CRT, and $Nlrp3^{A350V}/BRP^{-/-}$ CRT murine bone marrow isolated neutrophils by stimulating with recombinant IL8 and measuring the number of neutrophils migrating through a Transwell insert (3 $\mu\text{mol/L}$) over 2 hours (experimental design shown in Figure 7C). We found that NLRP3 activation significantly increased neutrophil migration ($P < .01$) in $Nlrp3^{A350V}$ CRT mice compared with WT control, and when BRP39 is conditionally deleted during NLRP3 activation, the chemotaxis ability of neutrophils is impaired drastically in $Nlrp3^{A350V}/BRP^{-/-}$ CRT mice compared with $Nlrp3^{A350V}$ CRT and WT mice ($P < .0001$) (Figure 7D). We performed the same experiment and confirmed the migration impairment phenomenon also has been observed in neutrophils from $BRP39^{-/-}$ CRT mice (Figure 7F). Interestingly, when $BRP39^{-/-}$ CRT neutrophils are pretreated overnight with 1 μg rmChi3L1 (Figure 7E), they responded to IL8 and migratory

function is restored to levels comparable with WT neutrophils.

Altogether, our data showed that BRP39 deficiency in NLRP3-activated mice increased the total circulating neutrophils (Figure 7A and B), but affected the migration ability (Figure 7D) of neutrophils to the site of inflammation, and this led to reduced accumulation and activation of neutrophils in the liver. In addition, pretreatment with recombinant Chi3L1 rescued IL8-dependent migratory function (Figure 7F), revealing the pivotal role of BRP39 in determining the chemotactic function of neutrophils.

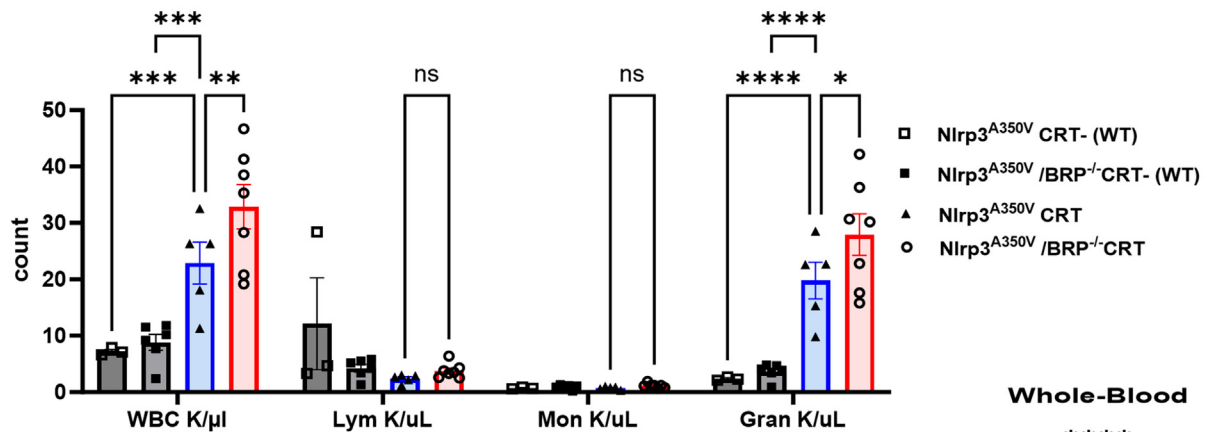
BRP39 Deficiency in NLRP3-Activated Neutrophils Showed Reduction in Immune Activation and Signaling Response

To understand the mechanistic role of BRP39 in NLRP3 inflammation, we performed RNA bulk sequencing of isolated neutrophils from whole-blood of $Nlrp3^{A350V}/BRP^{-/-}$ CRT mice and $Nlrp3^{A350V}$ CRT mice. We detected 53 up-regulated and 213 down-regulated genes that showed more than 2-fold change in mRNA expression (Figure 8A). The distinct pattern of gene expression generated from the top 25 differentially expressed genes is presented as a heatmap (Figure 8B), showing BRP39 deficiency during NLRP3 activation correlates with down-regulated expression of migration (Membrane alanyl aminopeptidase, Anpep) and complement C1 complex (C1qa and C1qb)-related genes when compared with NLRP3-activated neutrophils. Gene Ontology analysis of the Biological Processes-related pathways showed increased expression of genes associated with cell cycle and metabolism, meanwhile genes associated with immune response, signaling and cell aggregation such as complement activation, NF- κ B activation, and cell-junction assembly were down-regulated (Figure 8C). Taken together, the RNA sequencing data showed that BRP39 is important not only for neutrophil chemotaxis, but also dictates the activation and influences subsequent recruitment cascade of neutrophils from vasculature to tissue (Figure 9).

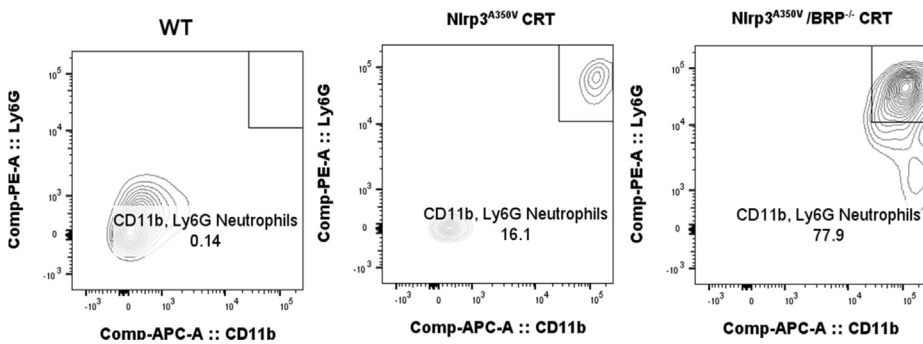
Discussion

The central findings of this study relate to how the absence of BRP39 could hinder the progression of NLRP3 inflammasome activation, liver injury, and fibrosis, and its implications in NASH. These results showed that deleting BRP39 in an inflammatory state mediated by NLRP3 inflammasome activation could improve the outcome of severe liver inflammation and fibrogenesis, characterized by reduced infiltration and accumulation of activated macrophages and neutrophils, subsequently lowering HSC activation and collagen deposition in the liver. These effects were partially mediated through the diminished expression of pro-caspase-1 and caspase-1 expression, thus reducing the downstream cascade of NLRP3 inflammasome activation, affecting downstream signaling, decreasing infiltration of activated bone marrow-derived mononuclear cells. BRP39 knockout in NLRP3-activated mice resulted in impairment of neutrophil chemotaxis, affecting signaling

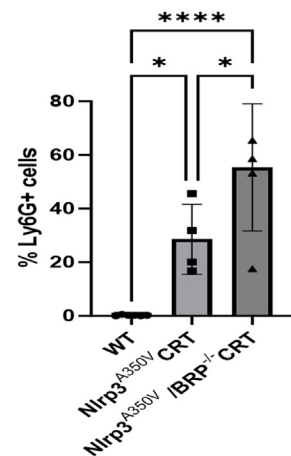
A Hematology Analysis



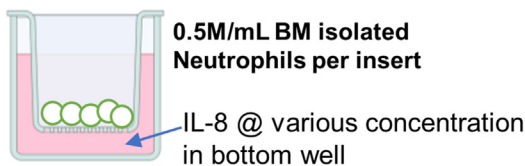
B



Whole-Blood



C

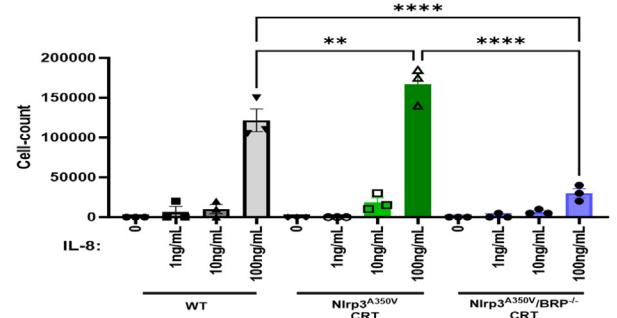


-Cells are left for 2 hours in the 37°C incubator

-After 2 hours, inserts are removed, and cells are collected from the bottom of the well, stained with trypan blue and counted with a hemocytometer

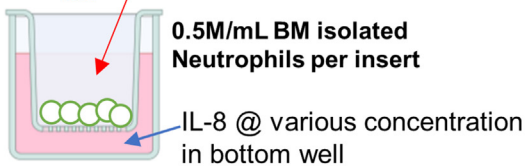
D

BM Neutrophil Chemotaxis-assay



E

Pre-treatment with Recombinant murine Chi3L1 O/N

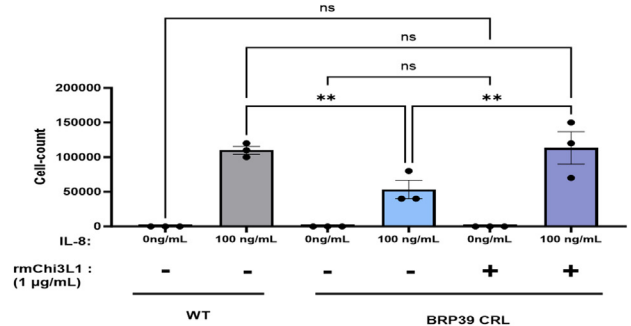


-Cells are left for 2 hours in the 37°C incubator

-After 2 hours, inserts are removed, and cells are collected from the bottom of the well, stained with trypan blue and counted with a hemocytometer

F

BM Neutrophil Chemotaxis-assay



and recruitment and cascade of infiltrating cells from circulation to the liver, leading to a drastic reduction of activated neutrophil accumulation in the liver. Our results identify BRP39 as a potential therapeutic target for treatment of NLRP3 inflammasome-mediated liver injury and fibrosis.

Our data show that BRP39 knockout dampens the effect of hyperactivation of NLRP3 inflammasome by diminishing caspase-1 expression. Previously, our group showed that NLRP3 inflammasome activation causes caspase-1-induced hepatocyte pyroptosis, liver inflammation, and fibrosis.^{20,23} Our data show that the absence of BRP39 during NLRP3 activation would reduce caspase-1 activation drastically and consequently dampen the inflammatory gene expression in the liver (Figure 4). In particular, macrophages deficient in BRP39 would have a dampened inflammatory potential, as shown with LPS and nigericin-stimulated, myeloid-specific BRP39 knockout macrophages (Figure 4D), showing significantly decreased inflammatory gene expression compared with stimulated WT macrophages. Moreover, the chemoattractant ability also vastly is diminished, as seen in significantly reduced chemokines (CCL1, CCL2, and CCL5) and chemokine-receptor CCR2 expression (Figure 4E). Breyne et al²⁶ showed with a murine *Escherichia coli* infection model that blocking of caspase with pan caspase inhibitor on infected mammary cells would decrease BRP39 expression, and subsequently abate inflammatory cytokine production. In another study by Dela Cruz et al²⁷ using *Streptococcus pneumoniae*-infected BRP39-null mice, they found that BRP39 is required for the inhibition of caspase-1-dependent macrophage pyroptosis by restricting inflammasome activation in the lungs. Our finding contributes toward the understanding of how BRP39 regulates NLRP3 inflammasome-mediated organ injury in the microenvironment of the liver by using a specific mouse model in which the activation of NLRP3 and knocking-out of BRP39 occur only by tamoxifen induction. Moreover, we showed that activated macrophage infiltration, and LAM (fibrosis-associated macrophage) deposition is decreased vastly in BRP39-deficient NLRP3-activated mice, which contributes toward an improved liver phenotype. The precise molecular mechanism by which BRP39 modulates NLRP3 activation will require additional investigation, and the possibility of an indirect effect cannot be ruled out completely. It is possible that the reduction of inflammatory cytokines and chemoattractant in the *Nlrp3*^{A350V}/*BRP*^{-/-} CRT liver creates a less-inflamed environment, which curbed the infiltration, recruitment, and accumulation of activated macrophages.

As shown previously and confirmed in our current study, activation of the NLRP3 inflammasome leads to neutrophilia in the blood and tissues and high levels of inflammatory mediators in the serum.^{23,28,29} BRP39 has been associated with its chemoattractant properties, affecting neutrophil and macrophage migration.³⁰ In fact, several groups have shown, directly or indirectly, the effects of BRP39 on neutrophil chemotaxis to the injured organs, either increased in the lungs²⁷ in the *E coli*-infected BRP39-null mouse model or decreased in the breast tissue²⁶ when BRP39 expression was abated after pan caspase treatment. Our group has shown that in the absence of BRP39, Choline-deficient L-amino-defined diet (CDAA)-fed mice have improved liver phenotype, having significantly less neutrophil infiltration.³¹ In the current study, in accordance with the CDAA diet model, we found a significant decrease in activated neutrophil accumulation (Figure 6) in the livers of *Nlrp3*^{A350V}/*BRP*^{-/-} CRT. Further investigation confirms that the absence of BRP39 in NLRP3-activated mice impairs the migration ability of neutrophils (Figure 7D), and pretreatment with recombinant Chi3L1 restored the migration function (Figure 7F), as shown in *BRP*^{-/-} CRT neutrophils. RNA sequencing results comparing *Nlrp3*^{A350V}/*BRP*^{-/-} CRT and *Nlrp3*^{A350V} CRT murine whole-blood neutrophils suggest the regulatory role of BRP39 in immune activation, cellular aggregation, migration, and NF- κ B signaling (Figure 8). Interestingly, one of the top 25 detected genes, CD13 (Anpep) (Figure 8B), was found to be down-regulated in *Nlrp3*^{A350V}/*BRP*^{-/-} CRT circulating neutrophils compared with *Nlrp3*^{A350V} CRT. CD13 expression was enriched in proinflammatory monocytes and has been implicated in cell trafficking.³² Human neutrophils with aberrant CD13 expression have impaired cellular aggregation, migration,³³ and tumor necrosis factor- α -induced apoptosis.³⁴ Our current data, supported by these previous studies, suggest how neutrophil chemotaxis, activation, and apoptosis may be regulated by BRP39 and how CD13 could be implicated in NLRP3 inflammation. Liver sinusoidal endothelial cells (LSECs) also play an important role in facilitating and sustaining liver injury and inflammation by releasing proinflammatory mediators such as tumor necrosis factor- α , IL6, IL1, and CCL2,³⁵⁻³⁷ and adhesion molecules such as intercellular adhesion molecule 1, vascular cell adhesion molecule 1, and Vascular adhesion protein-1 (VAP-1),^{35,36,38} which aid in enhancing leukocyte infiltration.³⁹ In particular, dysfunctional LSECs promote recruitment of macrophages via activating Kupffer cells.^{40,41} The deficiency of BRP39 is highly likely to impact the signaling cascade of

Figure 7. (See previous page). BRP39 deficiency in NLRP3-activated mice have increased Ly6G+ CD11b+ neutrophils in whole blood, however, the chemotaxis ability of neutrophils was impaired. (A) Hematology analysis in whole blood showed a significant increase in white-blood cell (WBC) and granulocyte count of *Nlrp3*^{A350V}/*BRP*^{-/-} CRT compared with *Nlrp3*^{A350V} CRT mice. n = 6, 2-way analysis of variance. (B) Flow cytometry analysis confirmed the increase of CD11b+ Ly6G+ cells in *Nlrp3*^{A350V}/*BRP*^{-/-} CRT vs *Nlrp3*^{A350V} CRT, in negative selected neutrophils from murine whole blood. (D) Using the experimental set-up in panel C, the neutrophil chemotaxis assay showed an impairment of neutrophil migration in *Nlrp3*^{A350V}/*BRP*^{-/-} CRT mice. (F) With the experimental set-up in panel E, neutrophil chemotaxis was impaired in BRP39 CRT neutrophils, and pretreatment with 1 μ g recombinant mouse Chi3L1 (BRP39) protein restored the chemotaxis ability. n \geq 3 mice per group. Data are expressed as the means \pm SEM. *P < .05, **P < .01, ***P < .001, ****P < .0001, 1-way analysis of variance. BM, Bone marrow.

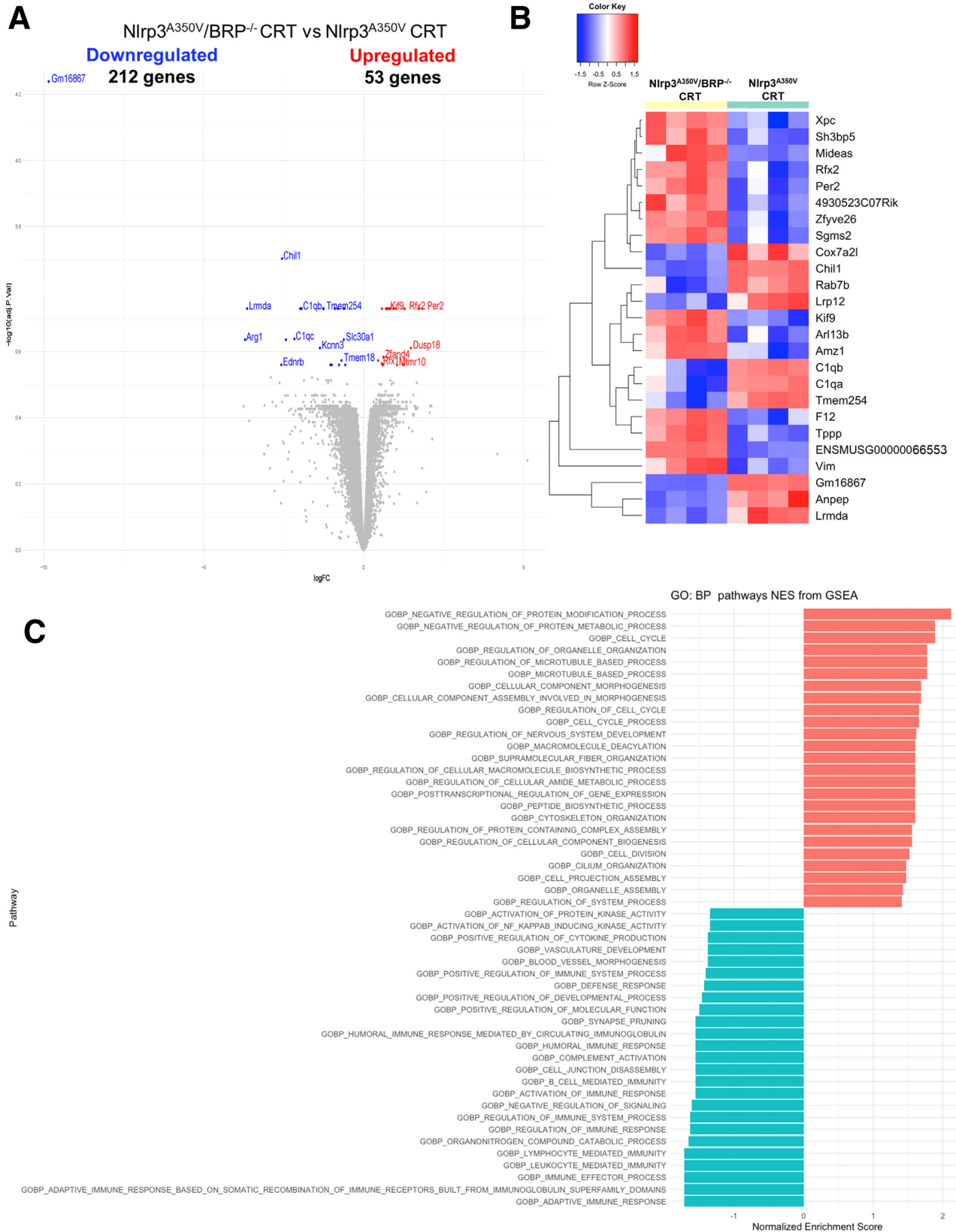


Figure 8. NLRP3-activated circulatory murine neutrophils with BRP39 deficiency have reduced immune activation, migration, and signaling response. (A) Volcano plot of up-regulated and down-regulated genes in isolated whole-blood murine neutrophils of Nlrp3^{A350V}/BRP^{-/-} CRT mice compared with Nlrp3^{A350V} CRT mice. (B) Heatmap representation of the top 25 genes after differential gene expression (DGE) analysis from RNA bulk sequencing of whole-blood neutrophils comparing Nlrp3^{A350V}/BRP^{-/-} CRT with Nlrp3^{A350V} CRT. (C) Gene Ontology (GO) Biological Process enrichment analysis of up-regulated (red) and down-regulated (blue) genes.

pathogenesis of liver inflammation and identifies BRP39 inhibition as a potential therapeutic strategy for treatment of NLRP3-mediated inflammatory diseases.

Methods

Mouse Strains

Tamoxifen-inducible *Nlrp3*^{A350V} CRT mice were generated as previously described.²² Briefly, conditional *Nlrp3*^{A350V} knockin mice were bred to the tamoxifen-inducible Cre-ER (CRT) B6.Cg-Tg (Cre/Esr1)5Amc/J mice (Jackson Laboratory) to allow for heterozygous mutant *Nlrp3* expression in adult models after administration of tamoxifen (*Nlrp3*^{A350V} CRT). Similarly, *Nlrp3*^{A350V} CRT mice deficient for BRP39 (*Nlrp3*^{A350V}/BRP^{-/-} CRT) were generated by crossing conditional BRP39 (Chi3L1) knockout mice³¹ to inducible *Nlrp3*^{A350V} CRT knockin mice, resulting in *Nlrp3*^{A350V}/BRP^{-/-} CRT mice that are heterozygous for the knockin allele and homozygous for the BRP39 knockout allele. Cre-negative mice were used as controls. BRP39 CRL mice also were generated by breeding conditional BRP39 knockout mice to mice expressing Cre recombinase under control of Lysozyme M Cre (LysMCre) or (CRL), myeloid lineage-specific knockout of BRP39, obtained from The Jackson Laboratory, Jax #004,781, B6.129P2-Lyz2tm1(cre)lfo/J. Littermates lacking the Cre recombinase were used as control mice.

Study Approval

The experimental protocol was approved by the Institutional Animal Care and Use Committee at the University of California San Diego.

NLRP3 Induction With Tamoxifen

For temporal induction of NLRP3 activation alone (*Nlrp3*^{A350V} CRT) or with BRP knockout (*Nlrp3*^{A350V}/BRP^{-/-} CRT), 7-week-old *Nlrp3*^{A350V} CRT, *Nlrp3*^{A350V}/BRP^{-/-} CRT, and WT were injected intraperitoneally with 50 mg/kg tamoxifen (cat# 156738; MPBio) reconstituted in 10% ethanol and 90% sunflower oil (S5007; Sigma) for 3 days (Figure 1A). Mice were cared for in accord with appropriate institutional guidelines. Experimental protocols were approved by the University of California San Diego (San Diego, CA) Institutional Animal Care and Use Committee.

Liver sample preparation. *Nlrp3*^{A350V} CRT, *Nlrp3*^{A350V}/BRP^{-/-} CRT, and WT mice were killed 3 weeks after tamoxifen induction. Liver tissue was harvested with representative pieces either (1) fixed in formalin for 24 hours, (2) placed in 0.5 mL RNA-later solution (cat# AM7020; Life Technologies Corporation), or (3) snap-frozen in liquid nitrogen and embedded in Tissue-Tek O.C.T. Compound (Cat#: 4583; Sakura) and stored at -80°C.

Bone marrow-derived macrophage generation and NLRP3 activation. Bone marrow cells were collected by flushing tibia and femurs with complete medium (CM) containing Dulbecco's modified Eagle medium, 1% GlutaMAX (cat# 35050061; Gibco), 1% penicillin-streptomycin, 1% nonessential amino acids, and 10% fetal bovine serum (FBS). Bone marrow aspirate was filtered through a 40- μ m mesh and centrifuged at 1500 rpm for 8 minutes at room

temperature. The cell pellet was resuspended with CM, plated at 2×10^6 /cm² on a 10-cm dish, and differentiated into macrophages with 10 ng/mL macrophage colony stimulating factor (recombinant mouse M-CSF, #576402; BioLegend) for 6 days (with 50% medium change on day 2 and 70% medium change on day 5) at 37°C, 5% CO₂, and 85%–98% humidity. On day 6, CM was aspirated and washed once with phosphate-buffered saline (PBS). Macrophages were harvested with gentle scraping in CM, and replated at 5×10^5 cells/500 μ L on a 24-well plate. For NLRP3 activation, cells were treated with 500 ng/mL LPS for 3 hours, followed by 40 μ mol/L nigericin for 45 minutes, and lysed with TRIzol Reagent (cat# 15596026; Invitrogen) for subsequent RNA isolation and reverse-transcription quantitative PCR.

Neutrophil Isolation From Bone Marrow and Whole Blood

Whole blood (~0.5 mL) was obtained from cardiac puncture and collected in an EDTA tube (BD 365974; Fisher Scientific). Bone marrow was flushed with complete medium [reagents from Gibco: RPMI 1640 [cat# 11875135], 10% FBS [heat inactivated] [cat# 10438026], 1% penicillin-streptomycin [5000 U/mL] [cat# 15070063], 1% L-glutamine [200 mmol/L] [cat# A2916801]], and collected from excised tibia and femur. Samples were topped up to 10 mL and centrifuged at 1500 rpm for 8 minutes, followed by treatment with red blood cell lysis buffer (cat# 420301; BioLegend), and washed twice with PBS. Whole blood and bone marrow isolate were stained with the mouse neutrophil isolation kit (cat# 130-097-658; Miltenyi Biotec) according to the manufacturer's protocol, and passed through LS column (cat# 130-042-401; Miltenyi Biotec). Neutrophil purity was $\geq 95\%$ as assessed by fluorescence-activated cell sorter. Isolated neutrophils from whole blood were used for flow analysis, and bone marrow neutrophils were used for chemotaxis assay.

Hematology and Flow Analysis on Whole-Blood Samples

Approximately 0.1 mL whole blood collected in an EDTA tube was used for hematology analysis using Veterinary hematology analyzer Scil Vet abc. Isolated whole-blood neutrophils were stained with anti-mouse CD11b-APC (allophycocyanin) (cat# 101211; BioLegend) and anti-mouse Ly6G-PE (Phycoerythrin) (cat# 551461; BD Biosciences) according to the manufacturer's protocol, and measured by flow cytometry (BD FACS Canto II). Data were analyzed using FlowJo 10.8.1 software (Tree Star). Neutrophils were measured as CD11b- and Ly6G-expressing cells.

Liver Histology and Immunostaining

Livers were sliced in 4- μ m sections. Liver fibrosis was assessed with picrosirius red staining and quantified by digital image analysis with QuPath version 0.3.2.⁴² For picrosirius red staining, liver sections were incubated for 30 minutes at room temperature with an aqueous solution of saturated picric acid containing 0.1% Fast Green FCF (color index 42053) and 0.1% Direct Red 80 (MilliporeSigma). IHC staining for α -SMA (1:250,

Table 1. List of Primers Used for Quantitative PCR Gene Expression Analysis

Species	Gene	Primer identifier (TaqMan)
Mouse	<i>Acta2</i>	Mm00725412_s1
	<i>Tgfb1</i>	Mm01178820_m1
	<i>Ctgf</i>	Mm01192933_g1
	<i>Col1a1</i>	Mm00801666_g1
	<i>Timp1</i>	Mm01341361_m1
	<i>Nlrp3</i>	Mm00840904_m1
	<i>Cxcl1</i>	Mm04207460_m1
	<i>Cxcl2</i>	Mm00436450_m1
	<i>Casp1</i>	Mm00438023_m1
	<i>I11b</i>	Mm00434228_m1
	<i>BRP39</i>	Mm00657889_mH
	<i>CCL1</i>	Mm00441236_m1
	<i>CCL2</i>	Mm00441242_m1
	<i>CCL5</i>	Mm01302427_m1
	<i>CCR2</i>	Mm99999051_gH

cat# ab124964; Abcam), mouse anti-F4/80 (1:100, cat# 123106; BioLegend), rat anti-Ly6C (1:100, cat# ab15627; Abcam), and rat anti-Ly6G (cat# 14-5931-82; Invitrogen) was performed on formalin-fixed, paraffin-embedded livers. After deparaffinization and rehydration of tissue, they were stained with the respective primary antibodies diluted in Dako Antibody Diluent (cat# S0809; Agilent Dako) overnight at 4°C in a humid chamber. They were washed twice in TBS-T (1X Tris-Buffered Saline, 0.1% Tween 20 Detergent) for 5 minutes, and incubated with the ready-to-use horseradish peroxidase (HRP)-linked anti-rat secondary IgG antibody (ImmPRESS HRP reagents, cat# MP-7404; Vector Labs, Burlingame, CA) for 1 hour at room temperature. Color was developed with the 3,3'-diaminobenzidine tetra hydrochloride substrate kit (cat# 550880; BD Pharmingen), and nuclei were counterstained with Mayer's hematoxylin for 2 minutes, followed by dehydration with increasing ethanol concentrations. Staining was quantified in 5 randomly selected fields (10× or 20× magnification), imaged with a Nanozoomer 2.0HT slide Scanner microscope (Hamamatsu Photonics K.K., Hamamatsu, Japan) and an Olympus VS200 Slide Scanner. The total stained area was analyzed by selecting brown areas using an unchanged threshold value in the macro function of ImageJ (NIH, Bethesda, MD). Results were represented as the average of the percentage of total area occupied by positive cells per field in each specimen.

Immunofluorescence of Frozen Mouse Liver Sections

Frozen liver sections were washed twice with PBS and fixed with ice cold methanol for 10 minutes. Next, the cells were washed, permeabilized (0.1% Tween-20 in PBS, 30 minutes), blocked for 1 hour with 1% bovine serum albumin-PBS, and incubated at 4°C with mouse monoclonal anti-CD68 (1:100, cat# ab955-500; Abcam), rat anti-Ly6G (cat# 14-5931-82; Invitrogen), goat anti-OPN (1:100, cat# AF808; Biotechne R&D), and rabbit anti-histone H3 (citrulline R2 + R8 + R17) (1:100, cat# ab5103; Abcam) antibodies diluted in Dako Antibody Diluent (cat# S0809; Agilent Dako). After an overnight

incubation, cells were washed twice with PBS and treated with Alexa Fluor 488 goat anti-rat (1:1000, cat# A11006; Invitrogen), Alexa Fluor 488 goat anti-mouse (1:1000, cat# A11029), Alexa Fluor 568 donkey anti-goat (1:1000, cat# A11057), or Alexa Fluor 594 donkey anti-rabbit (1:1000, cat# A21207) for 1 hour at room temperature in the dark, followed by washing twice with PBS and 5 minutes of nuclei staining with 4',6-diamidino-2-phenylindole (1 mg/mL, cat# 62248; Thermo Scientific) diluted at 1:1000 in PBS.

Real-Time PCR

RNA was extracted from 30 mg whole liver tissue with TRIzol reagent (cat# 15596026; Invitrogen) and the Qiagen RNeasy Kit 250 (cat# NC9307831) according to the manufacturer's instructions. Purified RNA (1000 ng) was reverse-transcribed into complementary DNA with the qScript complementary DNA Synthesis Kit (Quantabio). The primers listed in Table 1 were used for reverse-transcription PCR. Target gene expression levels were calculated by normalization with *GAPDH* gene expression levels in each sample, followed by a comparative cycle threshold Ct method ($2^{-\Delta\Delta Ct}$).

Neutrophil Chemotaxis Assay

Isolated bone-marrow neutrophils (0.5×10^6 cells) were added to the upper chamber of the Transwell inserts (3- μ m pore size) (cat# 353492; Falcon), and recombinant IL8 (cat# 574202; BioLegend) was added at various concentrations (1 ng/mL, 10 ng/mL, 100 ng/mL) to the bottom well, containing neutrophil culture medium (reagents from Gibco: Dulbecco's modified Eagle medium [cat# 11965092], 10% FBS [heat inactivated] [cat# 10438026], 1% penicillin-streptomycin [5000 U/mL] [cat# 15070063], 1% L-glutamine [200 mmol/L] [cat# A2916801], Granulocyte colony stimulating factor (G-CSF) 10 ng/mL [cat# 752108; BioLegend]). After incubating the chambers for 2 hours at 37°C, the transmigrated cells were collected from the lower chamber, stained with Trypan blue, and counted in a hemocytometer.

Western Blot Analysis

Approximately 5 mg liver tissue was used for protein extraction with 300 μ L 1 × RIPA buffer (cat# 9806; Cell Signaling) and 1:100 protease inhibitor cocktail (cat# P8340; Sigma), and was mechanically lysed using beads and a shaker for 1 minute 30 seconds. Samples were kept at -80°C and thawed the next day, and centrifuged for 10 minutes at 10,000 rpm at 4°C. Supernatant was collected and the protein concentration was determined with the Pierce BCA protein assay kit (cat# 23225; ThermoScientific). A total of 10 μ g protein sample was loaded in sodium dodecyl sulfate with 3% mercaptoethanol, heated for 10 minutes at 95°C, stacked with Any kD Mini-PROTEAN TGX Precast Protein Gels (Bio-Rad) set at 80 V for 30 minutes, followed by resolution at 120 V until the end of the run. Tris-glycine-sodium dodecyl sulfate was used as the running buffer. Proteins were transferred from the gel onto a nitrocellulose membrane in a Trans Blot Turbo Transfer system (Bio-Rad) for 7 minutes at 25 V, using buffer from the Trans-Blot Turbo RTA Midi 0.2 μ m Nitrocellulose Transfer Kit (cat #

1704271; Bio-Rad), followed by blockage of membrane for 1 hour with Intercept (TBS) Blocking Buffer (cat# 927-60001; Li-Cor) at room temperature, with light shaking, and then incubated with the appropriate primary antibodies (anti-NLRP3), monoclonal antibody (Cryo-2) (1:1000, cat# AG-20B-0014-C100; AdipoGen), α -tubulin (1:1000, cat# T6199-100; Sigma), caspase-1 p10 (Casper-2) (1:1000, cat# AG-20B-0044-C100; AdipoGen), and anti-IL1 β (1:1000, cat# ab9787; Abcam) overnight at 4°C. Membranes were washed twice in TBS-Tween buffer and incubated with HRP-linked anti-mouse or rabbit IgG antibodies, respectively (1:15,000; Li-Cor), for 1 hour at room temperature. Protein bands were scanned with the Li-Cor Odyssey 9120 Infrared Imaging System and analyzed with Image Studio software.

RNA Sequencing

RNA bulk sequencing was performed by the University of California San Diego IGM Genomics Center using an Illumina NovaSeq 6000. Briefly, total RNA was isolated from whole-blood neutrophils using the Qiagen miRNeasy Mini Kit. All samples had >250 ng of input RNA and an RNA integrity number value ≥ 7.0 . Sequencing libraries were created using the IlluminaTruSeq Stranded mRNA preparation, which preferentially selects for mRNA by taking advantage of the polyadenylated tail. Libraries were sequenced using the Illumina NovaSeq S4 platform, with a sequencing protocol of 50 bp paired-end sequencing (run-type, PE100) and a total read depth of 25 Million reads per sample.

Statistics

Statistical analyses were performed with Graph Pad Prism (version 9; Graph Pad Software, Inc, La Jolla, CA). The significance of 2-group comparisons was determined with the 2-tailed Student *t* test. Significance of more than 2 groups was analyzed by 1-way analysis of variance, and 2-way analysis of variance where applicable. The significance level was set at $P < .05$ for all comparisons. Error bars represent means \pm SEM. Experiments were repeated at least 3 times, and assays were performed in duplicate.

References

1. Brunt EM, Wong VWS, Nobili V, et al. Nonalcoholic fatty liver disease. *Nat Rev Dis Primers* 2015;1:15080.
2. Bedossa P. Pathology of non-alcoholic fatty liver disease. *Liver Int* 2017;37:85–89.
3. Nobili V, Alisi A, Newton KP, Schwimmer JB. Comparison of the phenotype and approach to pediatric vs adult patients with nonalcoholic fatty liver disease. *Gastroenterology* 2016;150:1798–1810.
4. Younossi ZM. Non-alcoholic fatty liver disease - a global public health perspective. *J Hepatol* 2019;70:531–544.
5. Shingina A, DeWitt PE, Dodge JL, et al. Future trends in demand for liver transplant: birth cohort effects among patients with NASH and HCC. *Transplantation* 2019;103:140–148.
6. Nouredin M, Vipani A, Bresee C, et al. NASH leading cause of liver transplant in women: updated analysis of indications for liver transplant and ethnic and gender variances. *Am J Gastroenterol* 2018;113:1649–1659.
7. Kang M-J, Yoon CM, Nam M, et al. Role of chitinase 3-like-1 in interleukin-18-induced pulmonary type 1, type 2, and type 17 inflammation; alveolar destruction; and airway fibrosis in the murine lung. *Am J Respir Cell Mol Biol* 2015;53:863–871.
8. Nikota JK, Botelho FM, Bauer CMT, et al. Differential expression and function of breast regression protein 39 (BRP-39) in murine models of subacute cigarette smoke exposure and allergic airway inflammation. *Respir Res* 2011;12:39.
9. Xu Q, Chai S-j, Qian Y-y, et al. Breast regression protein-39 (BRP-39) promotes dendritic cell maturation in vitro and enhances Th2 inflammation in murine model of asthma. *Acta Pharmacol Sin* 2012;33:1525–1532.
10. He CH, Lee CG, Dela Cruz CS, et al. Chitinase 3-like 1 regulates cellular and tissue responses via IL-13 receptor $\alpha 2$. *Cell Rep* 2013;4:830–841.
11. Lee CG, Hartl D, Lee GR, et al. Role of breast regression protein 39 (BRP-39)/chitinase 3-like-1 in Th2 and IL-13-induced tissue responses and apoptosis. *J Exp Med* 2009;206:1149–1166.
12. Johansen JS. Studies on serum YKL-40 as a biomarker in diseases with inflammation, tissue remodelling, fibroses and cancer. *Dan Med Bull* 2006;53:172–209.
13. Johansen JS, Pedersen AN, Schroll M, et al. High serum YKL-40 level in a cohort of octogenarians is associated with increased risk of all-cause mortality. *Clin Exp Immunol* 2008;151:260–266.
14. Johansen JS, Jensen BV, Roslind A, Price PA. Is YKL-40 a new therapeutic target in cancer? *Expert Opin Ther Targets* 2007;11:219–234.
15. Montgomery TA, Xu L, Mason S, et al. Breast regression protein-39/chitinase 3-like 1 promotes renal fibrosis after kidney injury via activation of myofibroblasts. *J Am Soc Nephrol* 2017;28:3218–3226.
16. Shan Z, Liu X, Chen Y, et al. Chitinase 3-like-1 promotes intrahepatic activation of coagulation through induction of tissue factor in mice. *Hepatology* 2018;67:2384–2396.
17. Pizano-Martínez O, Yañez-Sánchez I, Alatorre-Carranza P, et al. YKL-40 expression in CD14⁺ liver cells in acute and chronic injury. *World J Gastroenterol* 2011;17:3830–3835.
18. Johansen JS, Christoffersen P, Møller S, et al. Serum YKL-40 is increased in patients with hepatic fibrosis. *J Hepatol* 2000;32:911–920.
19. Kumagai E, Mano Y, Yoshio S, et al. Serum YKL-40 as a marker of liver fibrosis in patients with non-alcoholic fatty liver disease. *Sci Rep* 2016;6:35282.
20. Wree A, McGeough MD, Peña CA, et al. NLRP3 inflammasome activation is required for fibrosis development in NAFLD. *J Mol Med (Berl)* 2014;92:1069–1082.
21. Calcagno DM, Chu A, Gaul S, et al. NOD-like receptor protein 3 activation causes spontaneous inflammation and fibrosis that mimics human NASH. *Hepatology* 2022;76:727–741.
22. Schuster-Gaul S, Geisler LJ, McGeough MD, et al. ASK1 inhibition reduces cell death and hepatic fibrosis in an Nlrp3 mutant liver injury model. *JCI Insight* 2020;5:e123294.

23. Wree A, Eguchi A, McGeough MD, et al. NLRP3 inflammasome activation results in hepatocyte pyroptosis, liver inflammation, and fibrosis in mice. *Hepatology* 2014; 59:898–910.
24. Kaufmann B, Kui L, Reza A, et al. Cell-specific deletion of NLRP3 inflammasome identifies myeloid cells as key drivers of liver inflammation and fibrosis in murine steatohepatitis. *Cell Mol Gastroenterol Hepatol* 2022;14:751–767.
25. Remmerie A, Martens L, Thoné T, et al. Osteopontin expression identifies a subset of recruited macrophages distinct from Kupffer cells in the fatty liver. *Immunity* 2020;53:641–657.e14.
26. Breyne K, Steenbrugge J, Demeyere K, et al. Immunomodulation of host chitinase 3-like 1 during a mammary pathogenic *Escherichia coli* infection. *Front Immunol* 2018;9:1143.
27. Dela Cruz CS, Liu W, He Chuan H, et al. Chitinase 3-like-1 promotes *Streptococcus pneumoniae* killing and augments host tolerance to lung antibacterial responses. *Cell Host Microbe* 2012;12:34–46.
28. Brydges SD, Mueller JL, McGeough MD, et al. Inflammasome-mediated disease animal models reveal roles for innate but not adaptive immunity. *Immunity* 2009; 30:875–887.
29. Bonar SL, Brydges SD, Mueller JL, et al. Constitutively activated NLRP3 inflammasome causes inflammation and abnormal skeletal development in mice. *PLoS One* 2012;7:e35979.
30. Sohn MH, Kang M-J, Matsuura H, et al. The chitinase-like proteins breast regression protein-39 and YKL-40 regulate hyperoxia-induced acute lung injury. *Am J Respir Crit Care Med* 2010;182:918–928.
31. Kim AD, Kui L, Kaufmann B, et al. Myeloid-specific deletion of chitinase-3-like 1 protein ameliorates murine diet-induced steatohepatitis progression. *J Mol Med* 2023;101:813–828.
32. Ghosh M, Gerber C, Rahman MM, et al. Molecular mechanisms regulating CD13-mediated adhesion. *Immunology* 2014;142:636–647.
33. Fiddler CA, Parfrey H, Cowburn AS, et al. The aminopeptidase CD13 induces homotypic aggregation in neutrophils and impairs collagen invasion. *PLoS One* 2016;11:e0160108.
34. Cowburn AS, Sobolewski A, Reed BJ, et al. Aminopeptidase N (CD13) regulates tumor necrosis factor- α -induced apoptosis in human neutrophils. *J Biol Chem* 2006;281:12458–12467.
35. Lefere S, Van de Velde F, Hoorens A, et al. Angiopoietin-2 promotes pathological angiogenesis and is a therapeutic target in murine nonalcoholic fatty liver disease. *Hepatology* 2019;69:1087–1104.
36. Miyachi Y, Tsuchiya K, Komiya C, et al. Roles for cell-cell adhesion and contact in obesity-induced hepatic myeloid cell accumulation and glucose intolerance. *Cell Rep* 2017;18:2766–2779.
37. Wu J, Meng Z, Jiang M, et al. Toll-like receptor-induced innate immune responses in non-parenchymal liver cells are cell type-specific. *Immunology* 2010; 129:363–374.
38. Weston CJ, Shepherd EL, Claridge LC, et al. Vascular adhesion protein-1 promotes liver inflammation and drives hepatic fibrosis. *J Clin Invest* 2015; 125:501–520.
39. Gao J, Wei B, Liu M, et al. Endothelial p300 promotes portal hypertension and hepatic fibrosis through C-C motif chemokine ligand 2-mediated angiocrine signaling. *Hepatology* 2021;73:2468–2483.
40. Hammoutene A, Rautou PE. Role of liver sinusoidal endothelial cells in non-alcoholic fatty liver disease. *J Hepatol* 2019;70:1278–1291.
41. Roh YS, Seki E. Chemokines and chemokine receptors in the development of NAFLD. *Adv Exp Med Biol* 2018; 1061:45–53.
42. Bankhead P, Loughrey MB, Fernández JA, et al. QuPath: open source software for digital pathology image analysis. *Sci Rep* 2017;7:16878.

Received July 26, 2023. Accepted December 6, 2023.

Correspondence

Address correspondence to: Ariel E. Feldstein, MD, Department of Pediatrics, University of California, San Diego, 3020 Children's Way, MC 5030, La Jolla, California 92103-8450. e-mail: afeldstein@ucsd.edu.

Acknowledgments

The authors thank Dr Ben A Croker for advice on the experimental design of the neutrophil migration study. The University of California San Diego Microscopy Core Nanozoomer 2.0 HT slide Scanner microscope was supported by Hamamatsu Photonics K.K., Hamamatsu, Japan, grant NS047101. The RNA sequencing analysis was supported by Altman Clinical and Translational Research Institute grant UL1TR001442.

CRedit Authorship Contributions

Lin Kui, PhD (Conceptualization: Lead; Data curation: Lead; Formal analysis: Lead; Investigation: Lead; Methodology: Lead; Writing – original draft: Lead)
 Andrea D Kim, MD (Investigation: Supporting; Methodology: Supporting)
 Janset Onyuru (Mouse breeding and colony maintenance: Supporting)
 Harold M Hoffman, MD (Funding acquisition: Equal; Resources: Equal; Supervision: Equal; Writing – review & editing: Equal)
 Ariel E Feldstein, MD (Funding acquisition: Equal; Resources: Equal; Supervision: Lead; Writing – review & editing: Equal)

Conflicts of interest

These authors disclose the following: Ariel E. Feldstein is an employee and stockholder of Novo Nordisk, and Hal M. Hoffman consults for Novartis. The remaining authors disclose no conflicts.

Funding

This work was funded by National Institutes of Health grants 5R01DK113592-05 (A.E.F and H.M.H), and R01 AI155869 and P01 HL152958 (H.M.H).